Hyperfine Interactions (2023) 244:24
https://doi.org/10.1007/s10751-023-01836-3

CONFERENCE PROCEEDING

^{193}Ir nuclear forward scattering of an iridium(I) complex

Maren H. Hoock[1] · Olaf Leupold[2] · Alexander Haag[3] · Andreas Omlor[1] · Rene Steinbrügge[2] · Ilya Sergueev[2] · Ralf Röhlsberger[2,4] · Hans-Jörg Krüger[3] · Juliusz A. Wolny[1] · Volker Schünemann[1]

Accepted: 20 November 2023
© The Author(s) 2023

Abstract
Synchrotron based nuclear forward scattering (NFS) experiments using the ^{193}Ir nucleus have been performed for the first time on a dinuclear iridium(I) complex, $[IrCl(COD)]_2$ with COD being cycloocta-1,5-diene. This complex serves as a catalyst for hydrogenation and other chemical reactions. Both, the obtained absolute values of the isomer shift $\delta = 0.87$ mm s^{-1} and the quadrupole splitting $\Delta E_Q = 3.82$ mm s^{-1} agree within the experimental error with values obtained via conventional ^{193}Ir Mössbauer spectroscopy reported earlier (Gál M. et al. J. Radioanal. Nucl. Chem., 260 (1) 2004, 133). In addition, we present density functional theory (DFT) calculations of the complex yielding its electronic structure and related Mössbauer parameters.

Keywords ^{193}Ir nuclear forward scattering · ^{193}Ir Mössbauer spectroscopy · Density functional theory · Iridium complexes

1 Introduction

Mössbauer spectroscopy using the 73 keV transition from the I = 3/2 ground to the I = 1/2 first excited state of ^{193}Ir has been considered as an optimal method to study hyperfine interactions in iridium containing materials because of its low natural line width of 0.625 mm s^{-1} [1]. However, ^{193}Ir Mössbauer spectroscopy requires ^{193}Os as a radioactive source which has a half life time of 31d and needs to be prepared via neutron irradiation by a ^{192}Os(n,γ)^{193}Os reaction [2, 3]. This has hampered more widespread applications of ^{193}Ir Mössbauer spectroscopy in the past although the ^{193}Ir isotope has a high natural abundance of 62%.

✉ Volker Schünemann
schuene@rptu.de

1 Department of Physics, RPTU Kaiserslautern-Landau, Erwin-Schrödinger-Str. 46, 67663 Kaiserslautern, Germany

2 Deutsches Elektronen Synchrotron (DESY), Notkestr. 85, 22607 Hamburg, Germany

3 Department of Chemistry, RPTU Kaiserslautern-Landau, Erwin-Schrödinger-Str. 52, 67663 Kaiserslautern, Germany

4 Helmholtz Institut Jena and Friedrich-Schiller Universität Jena, Max-Wien-Platz 1, 07743 Jena, Germany

Published online: 05 December 2023

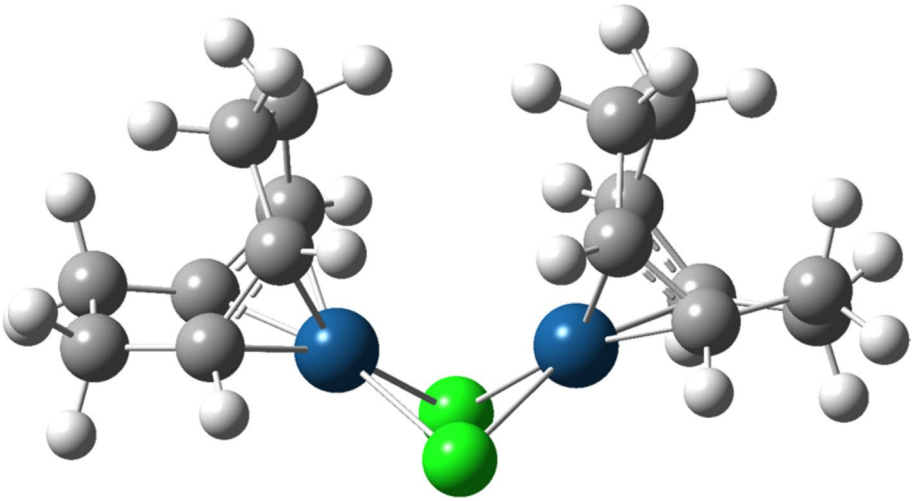

Fig. 1 Structural view of the dinuclear iridium(I) complex $[IrCl(COD)]_2$ investigated in this study. Ir atoms are displayed in dark blue, chloride atoms in green, carbon atoms in dark grey and hydrogens in grey [11]

The high brilliance at modern synchrotron sources and the recent development of monochromator systems for 73 keV with an energy resolution of 160 meV at the Dynamics Beamline P01 (PETRA III, DESY, Hamburg) now enables to excite the 73 keV level from the ground state to perform coherent nuclear forward scattering (NFS) experiments using the ^{193}Ir nucleus. This set-up has been developed and used by Alexeev et al. [4] for the studies of magnetic and electronic properties of iridates which display both strong spin orbit coupling and strongly correlated electron systems.

Iridium containing materials play an important role in chemistry. For example, in photochemistry molecular iridium complexes are used in organic light-emitting diodes (OLEDs) [5, 6], organic solar cells [7], in photocatalysis [8], in car exhaust catalysts but also recently for initiating "*water oxidation reactions* " [9, 10]. In this process water is catalytically split into hydrogen and oxygen, a prerequisite to enable hydrogen as a sustainable storable energy source.

Here, we report the first ^{193}Ir NFS experiments on a molecular material, namely a dinuclear iridium(I) complex, $[IrCl(COD)]_2$ [11] with COD being cycloocta-1,5-diene (Fig. 1). This complex serves as a catalyst for hydrogenation and other chemical reactions [12–22]. It has been investigated by conventional ^{193}Ir Mössbauer spectroscopy in the past [23, 24] which makes this system ideal for elucidating the potential of ^{193}Ir NFS with respect to its chemical applications. In addition, we present density functional theory (DFT) calculations, which have been used to calculate the isomer shift and the quadrupole splitting of the dinuclear iridium(I) complex.

2 Materials and methods

Di-μ-chlorobis[(1,2,5,6-η)-1,5-cyclooctadiene]diiridium ($C_{16}H_{24}Cl_2Ir_2$; CAS No.: 12112-67-3) was synthesized as described in [25]. For ^{193}Ir NFS experiments the sample was filled in a hole with a diameter of 2 mm and a length of 4 mm of a sample

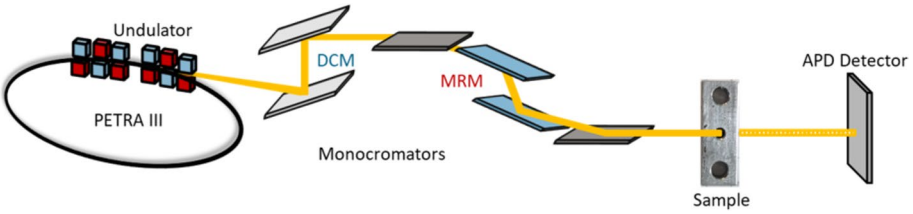

Fig. 2 Set-up for ^{193}Ir NFS at beamline P01, PETRA III: DCM - double crystal monochromator consisting of Si (311) single crystals (grey); MRM - medium resolution monochromator consisting of Si(422) (blue) and Si(800) (dark grey) single crystals

holder made of aluminium. The sample was tightly pressed into the sample volume and sealed with aluminium tape.

^{193}Ir NFS experiments were performed at the Dynamics Beamline P01 (PETRA III, DESY, Hamburg) using the 40-bunch mode with a time separation of 192 ns between the electron bunches of the PETRA III storage ring.

The synchrotron radiation (SR) generated by the undulator source was monochromatized with a double-crystal monochromator (DCM) consisting of two Si(311) crystals (see Fig. 2) to about 10 eV. The medium resolution monochromator (MRM) reduced the energy bandwidth to about 160 meV. The MRM consisted of two asymmetric channel-cut silicon crystals, a Si(422) collimator crystal and a Si(800) energy selector crystal. Subsequently, the SR, monochromatized to 73.0 keV, was transmitted through the sample mounted in a He-closed cycle cryostat from Advanced Research Systems, Inc. The delayed resonantly scattered radiation was detected with an avalanche photo diode (APD) detector array. The APD detector allowed a time resolution of ~0.6 ns and ^{193}Ir-NFS time spectra could be obtained as early as 3 ns after the excitation by the SR pulses by using time gated electronics.

For the determination of the quadrupole splitting (ΔE_Q) and the isomer shift (δ) the ^{193}Ir-NFS data were analyzed with the CONUSS software [26] as described in Alexeev et al. [4].

DFT calculations were used to calculate the hyperfine parameters δ and ΔE_Q on the basis of the crystal structure of $[IrCl(COD)]_2$ [11]. Structure optimization and Natural bond orbital (NBO) analysis [27] was performed with *Gaussian 16* [28] using Grimme's dispersion with the original D3 damping function [29] for the functional *TPSSTPSS* and the basis set *QZVP* [30, 31]. Kohn-Sham Molecular orbitals (MOs) and their energies were calculated and graphically represented by the *Gauss View* mode.

With the optimized structures, calculations of the hyperfine parameters were performed using the *Orca 5.0* programme [32]. For this purpose, all-electron calculations of the *SARC* (segmented all-electron relativistically contracted) basis sets were used, which have been specially developed for scalar relativistic calculations and have been adapted to the Douglas-Kroll-Hess Hamiltonian of the second order (*DKH2*) [31]. The *DKH-def2-TZVP* basis set [30] was used for C, H, F, Br and Cl and the *SARC-DKH-TZVP* basis set [33] was used for the two Ir atoms. Calculations were performed with

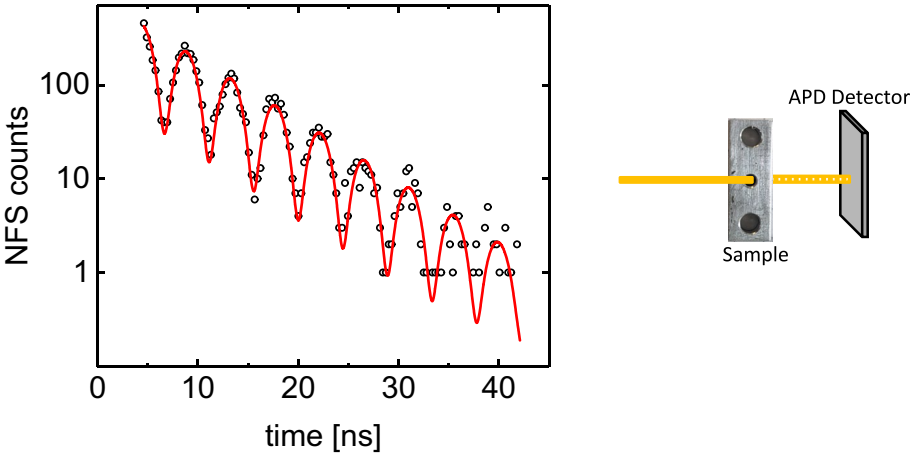

Fig. 3 ^{193}Ir NFS spectrum of $[IrCl(COD)]_2$ obtained at 10 K (black circles) (left) with the APD detector mounted behind the sample inside a closed cycle cryostat (right). The red line is a simulation performed with CONUSS [20] yielding $\Delta E_Q = 3.82(4)$ mm s^{-1}

both *TPSS* and *B3LYP* functionals. The convergence criteria and grid points for the self-consistent field (*SCF*) calculations were set to *Tight SCF* (energy change $1 \cdot 10^{-8} au$). All SCF calculations were performed with the resolution of the Identity Approximation (*RI*) [34]. The programme *Orca_eprnmr* implemented in *Orca* was used to calculate the electron density ρ_0 and the electric field gradient (EFG) tensor at the iridium core [34].

3 Results and discussion

Figure 3 shows a ^{193}Ir NFS spectrum of $[IrCl(COD)]_2$ obtained at T = 10 K. The spectrum shows a beating pattern with a time period of about 5 ns which originates from the non-zero EFG of the two equivalent Ir sites in $[IrCl(COD)]_2$. The beating pattern could be successfully reproduced by a simulation with CONUSS which gave $\Delta E_Q = 3.82(4)$ mm s^{-1}. There are small deviations between experimental and simulated data occurring at >25 ns which may be due by some spurious bunches of the synchrotron. Nevertheless, the so obtained value of the quadrupole splitting is in excellent agreement with those obtained by conventional ^{193}Ir Mössbauer spectroscopy for this complex at liquid He temperatures (3.81(2) mm s^{-1} [23] and 3.85(2) mm s^{-1}, respectively [24]).

For the determination of the isomer shift a data set with a metallic iridium foil as a single-line reference was collected. The corresponding ^{193}Ir NFS spectrum is shown in Fig. 4. The interference of the 73 keV resonantly scattered quanta originating from the iridium foil and the $[IrCl(COD)]_2$ sample leads to the disappearance of the regular beating structure visible in Fig. 3. A simulation with CONUSS using two Ir sites with $\Delta E_Q = 3.82$ mm s^{-1} representing $[IrCl(COD)]_2$ and $\Delta E_Q = 0$ mm s^{-1} for the metallic Ir foil yields $\delta = \pm 0.87(4)$ mm s^{-1} for the complex. It is important to note that the sign of δ cannot be obtained using the set-up displayed in Fig. 4. Indeed, conventional ^{193}Ir Mössbauer spectroscopy showed that the sign of the isomer shift of $[IrCl(COD)]_2$ is negative. Nevertheless, the absolute δ-value obtained in this study is in excellent agreement with the reported values of $-0.88(1)$ mm s^{-1} [23] and $-0.87(1)$ mm s^{-1} [24].

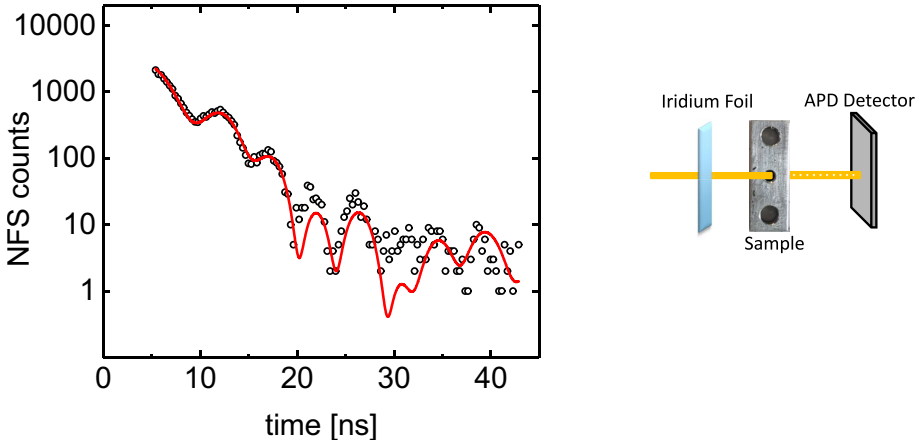

Fig. 4 ^{193}Ir NFS spectrum of $[IrCl(COD)]_2$ obtained at 10 K (black circles) (left) with an iridium foil mounted in the beam path (right). Temperature of the iridium foil was 300 K. The red line is a simulation performed with CONUSS [20] using $\Delta E_Q = 3.82(4)$ mm s^{-1} for the Ir sites of $[IrCl(COD)]_2$ yielding $\delta = 0.87(4)$ mm s^{-1} for the complex

It has been shown by [35] that experimentally observed isomer shifts are related to the theoretically calculated electron density at the iridium nucleus ρ_0^{calc} via the following relation:

$$\delta = a\left(\rho_0^{calc} - b\right) + c$$

The parameters a, b and c are fit parameters which need to be obtained from a series of complexes with known experimental values of δ and calculated ρ_0^{calc} which can be obtained by DFT methods based on known molecular structures. For ^{57}Fe containing complexes this approach has been shown by various authors to be very successful [36, 37] The same strategy has been used recently within the frame of a DFT study to calculate ^{193}Ir Mössbauer spectroscopic parameters [34].

For the determination of ρ_0^{calc} of the complex $[IrCl(COD)]_2$ investigated in this study DFT calculations of the various iridium(I), iridium(III) and iridium (IV) complexes listed in ref. [34] were repeated with the *Orca 5.0* programme [32] as described in the Materials and Methods section. Table 1 provides a list of the iridium complexes and experimental δ values and lists the charge and multiplicity of the complexes used for the calculations. The Cartesian coordinates of the complexes were taken from [34]. Our DFT calculations performed with both, the functional *TPSS* and *B3LYP* gave slightly differentρ_0^{calc} values than reported in ref. [34] (Table 1) and were used to perform a linear regression analysis between ρ_0^{calc} and measured δ values as shown for both functionals in Fig. 5. For $[IrCl(COD)]_2$ we obtain electron densities at the iridium core of 2657326.5773 au^{-3} when using *TPSS* and 2658125.7642 au^{-3} when using *B3LYP*. With the parameters a, b and c given in Table 2 the calculated isomer shifts for the complex are $\delta_{TPSS} = -0.58$ mm s^{-1} and $\delta_{B3LYP} = -0.65$ mm s^{-1}. Although the absolute values of

Table 1 Experimental isomer shifts δ of iridium complexes listed in ref. [2, 23, 24, 34, 38] and calculated electron densities at the iridium nucleus ρ_0^{calc} obtained by DFT calculations performed in this study with the functionals *TPSS* and *B3LYP*

Complex	δ [mm s^{-1}]	Ref.	Charge	Multiplicity	$\rho^{calc}_{0_{TPSS}}$ [au^{-3}]	$\rho^{calc}_{0_{B3LYP}}$ [au^{-3}]
$[Ir^{III}Br_6]^{3-}$	-2.23(3)	[2]	-3	1	2657283.0545	2658084.3623
$[Ir^{III}Cl_6]^{3-}$	-2.26(3)	[2]	-3	1	2657280.9270	2658082.1558
trans-$[Ir^{III}Cl_4(py)_2]^-$	-1.73(3)	[38]	-1	1	2657305.2701	2658105.3922
$[Ir^{III}(SCN)_6]^{3-}$	-1.65(3)	[38]	-3	1	2657306.0747	2658107.5108
$[Ir^{III}(NH_3)_6]^{+3}$	-1.51(2)	[38]	+3	1	2657300.3303	2658100.6602
$[Ir^{III}(CN)_6]^{3-}$	0.26(1)	[2]	-3	1	2657336.2254	2658137.5882
$[Ir^{IV}Br_6]^{2-}$	-1.10(2)	[2]	-2	2	2657306.4264	2658110.7226
$[Ir^{IV}Cl_6]^{2-}$	-0.95(2)	[2]	-2	2	2657307.8814	2658112.2327
trans-$[Ir^{IV}Cl_4(py)_2]$	-0.67(2)	[38]	0	2	2657321.8203	2658125.4879
trans-$[Ir^{I}Br(CO)(Phh_3)_2]$	0.010(15)	[34]	0	1	2657345.5671	2658144.8336
trans-$[Ir^{I}Cl(CO)(Phh_3)_2]$	-0.06(10)	[34]	0	1	2657346.4855	2658145.7629
trans-$[Ir^{I}F(CO)(Phh_3)_2]$	0.28(10)	[34]	0	1	2657349.7936	2658148.8378
trans-$[Ir^{III}Cl(Cl)_2(CO)(Phh_3)_2]$	-0.480(15)	[34]	0	1	2657330.2666	2658132.1362
trans-$[Ir^{III}Cl(O_2)(CO)(Phh_3)_2]$	-0.290(15)	[34]	0	1	2657332.8288	2658134.4527
trans-$[Ir^{III}Cl(H)(Cl)(CO)(Phh_3)_2]$	0.240(15)	[34]	0	1	2657346.8556	2658148.5975
trans-$[Ir^{III}Cl(H)_2(CO)(Phh_3)_2]$	0.350(15)	[34]	0	1	2657348.3391	2658149.9957
$[Ir^{I}Cl(COD)]_2$	-0,87(1) -0,88(1)	[24] [23]	0	1	2657326.5773	2658125.7642

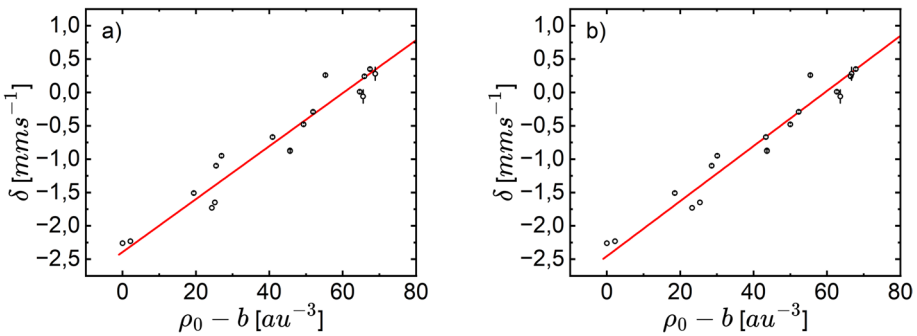

Fig. 5 Experimental δ -values as a function of calculated ρ_0-values for the *TPSS* (**a**) and *B3LYP* (**b**) functionals. The black points represent the experimental data (Table 1) and the red line the result of a linear regression analysis with parameters *a*, *b* and *c* listed in Table 2

the calculated isomer shifts are below the experimental value of $\delta = -0.87$ mm s^{-1} the DFT calculations also give a negative sign of the isomer shift as has been observed by conventional ^{193}Ir Mössbauer spectroscopy.

The DFT calculations performed in this study also deliver the main components of the EFG tensor V_{xx}, V_{yy} and V_{zz} in its principal axis system ($|V_{xx}| \leq |V_{yy}| \leq |V_{zz}|$). With

Table 2 Parameters of the linear regression analysis shown in Fig. 5 for the *TPSS* and *B3LYP* functionals

	TPSS	*B3LYP*
a[mm s^{-1}au^{-3}]	0,040(4)	0,041(3)
b[au^{-3}]	2,657,281	2,658,082
c[mm s^{-1}]	-2,393(216)	-2,454(184)
R^2	0,83793	0,8841

R^2 represents goodness of fit

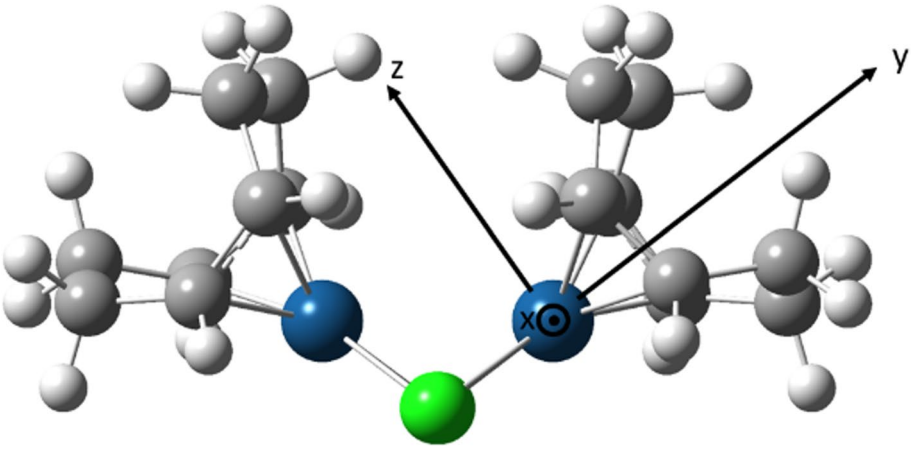

Fig. 6 Coordinate axes system of the electronic orbitals of the right iridium atom of the complex chosen from the symmetry axis of the d_{z^2} orbital. Note that inversion of the z-axis would interchange the x and y axes. The latter were chosen from the symmetry axes of the p orbitals

the asymmetry parameter $\eta = (V_{xx} - V_{yy})/V_{zz}$ and the quadrupole moment Q the quadrupole splitting is given as:

$$\Delta E_{Q_{exp}} = \frac{eQV_{zz}}{2}\sqrt{1+\frac{\eta^2}{3}}$$

Taking $Q = 0.751$ b for the first excited nuclear state of ^{193}Ir and the expression $eQV_{zz}\left[mm\ s^{-1}\right] = (eQV_{zz}[J] \times c\left[mm\ s^{-1}\right])/E_{\gamma}[J]$ with the speed of light c in units of $mm\ s^{-1}$ allows to obtain ΔE_Q in its usual units since the DFT package ORCA delivers the EFG tensor components in units of *au*.

In this way we obtained for both functionals *TPSS* and *B3LYP* a positive sign of the quadrupole splitting and slightly different absolute values of $\Delta E_Q^{B3LYP} = +4.70$ mm s^{-1}; $\eta^{B3LYP} = 0.29$ and $\Delta E_Q^{TPSS} = +4.25$ mm s^{-1}; $\eta^{TPSS} = 0.43$. Giving the fact that for quadrupole splittings of ^{57}Fe containing compounds deviations between experimental and DFT calculated ΔE_Q values in the order of ~ 1 mm s^{-1} are not uncommon [39] we consider the agreement with the experimental value of $\Delta E_Q = 3.82$ mm s^{-1} at least for the complex [IrCl(COD)]$_2$ investigated here as reasonable.

Gal et al. [24] argued that $\delta = -0.87$ mm s^{-1} of [IrCl(COD)]$_2$ is unusually high compared to other Ir(I) complexes which show typically $\delta \sim -4$ mm s^{-1}. They attributed this to a σ donation into the 6s orbitals as well as hybridization of the 6s with the $5d_{z^2}$ orbitals.

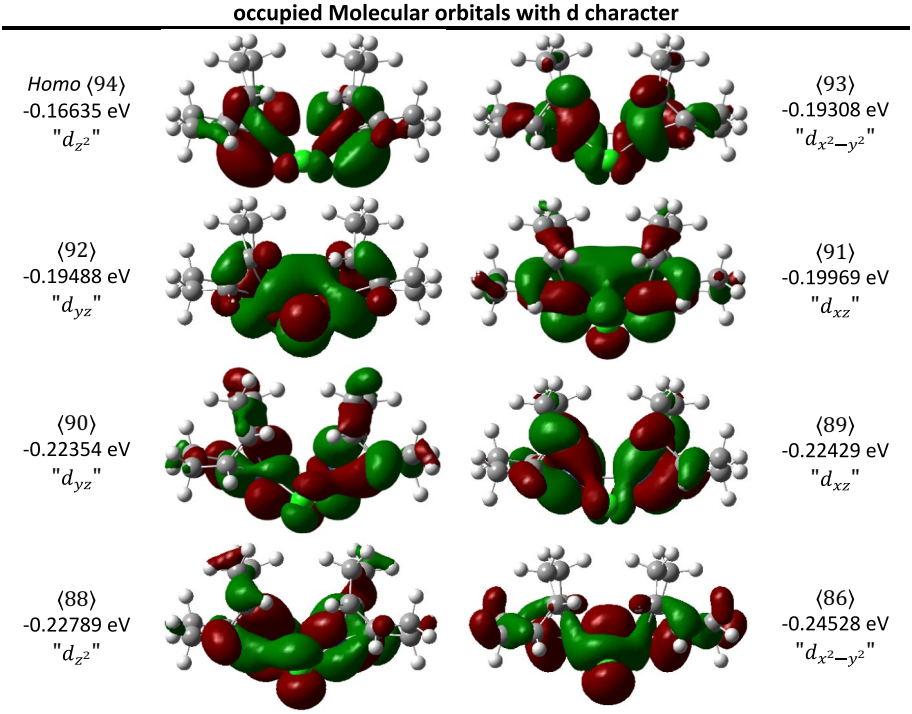

Fig. 7 DFT calculated Kohn-Sham molecular orbitals with 5d character obtained from the optimized structure of $[IrCl(COD)]_2$. Numbers in brackets represent the number of the molecular orbitals as given in the output-file of Gaussian16

According to our NBO analysis, the electron configuration of the iridium is 6s(0.48)5d(8.02)6p(0.32)7p(0.19). The eight occupied MOs with 5d character according to the reference frame given in Fig. 6 are shown in Fig. 7. Our calculations indicate that the 5p and 5s-orbitals prevail their character as expected (Fig. 8).

The DFT calculations presented here show a positive V_{zz} which is in contradiction with the reported presumably negative V_{zz} assumed by Gal et al. [24]. Future experimental investigations with NFS experiments in high external fields can serve to determine the sign of the quadrupole splitting and may shine more light on the binding properties of catalytically active iridium complexes.

4 Conclusions

In this work it has been shown that the ^{193}Ir NFS is an excellent alternative to conventional ^{193}Ir Mössbauer spectroscopy. Moreover, we have shown that it is possible to calculate Mössbauer parameters like the isomer shift and the quadrupole splitting using state of the

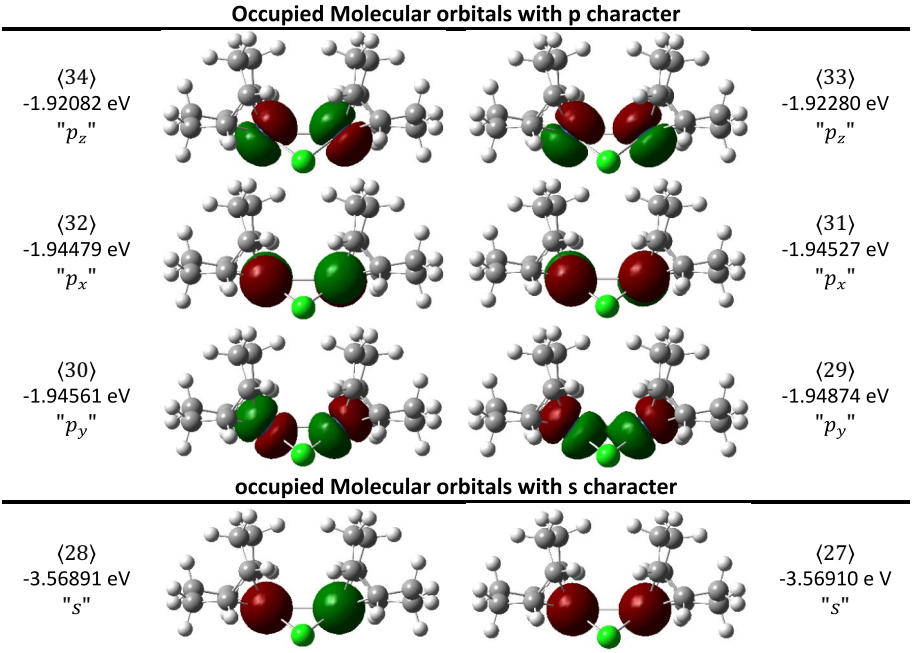

Fig. 8 DFT calculated Kohn-Sham molecular orbitals with 5p and 5s character obtained from the optimized structure of $[IrCl(COD)]_2$. Numbers in brackets represent the number of the molecular orbitals as given in the output-file of Gaussian16

art DFT methods with satisfying accuracy. The combination of experimental ^{193}Ir NFS and quantum chemical DFT methods may represent an important technique for future characterisation of the magnetic and electronic properties of iridium containing molecular systems.

Supplementary Information The online version contains supplementary material available at https://doi.org/10.1007/s10751-023-01836-3.

Acknowledgements V.S. and H.J.K acknowledge the support by the Deutsche Forschungsgemeinschaft (DFG) through CRC/TRR88, "Cooperative Effects in Homo-and Hetero-Metallic Complexes(3MET)" and through CRC/TRR173 "Spin+X" (V.S.). V.S. also acknowledges support by the CRC/ German Federal Ministry of Education and Research (BMBF) under 05K22UK1.

Author contributions M.H.H. and V.S. wrote the main manuscript text. O.L., R.S., and I.S. performed the NFS experiments. O.L. and M.H.H. performed data analysis. J.W. and M.H.H. performed DFT calculations. R.R. and V.S. wrote application for beamtime. A.O., A.H. and H.J.K. provided the sample. All authors reviewed the manuscript.

Funding Open Access funding enabled and organized by Projekt DEAL. Deutsche Forschungsgemeinschaft (DFG): CRC/TRR88, "3MET", Project A04; CRC/TRR173 "Spin+X", Project A04.
German Federal Ministry of Education and Research (BMBF): Project 05K22UK1.

Data availability Any data is available on request to either the first or the communicating author.

Declarations

Ethical approval N.A., no human and/ or animal studies.

Competing interests The authors declare no competing interests.

Open Access This article is licensed under a Creative Commons Attribution 4.0 International License, which permits use, sharing, adaptation, distribution and reproduction in any medium or format, as long as you give appropriate credit to the original author(s) and the source, provide a link to the Creative Commons licence, and indicate if changes were made. The images or other third party material in this article are included in the article's Creative Commons licence, unless indicated otherwise in a credit line to the material. If material is not included in the article's Creative Commons licence and your intended use is not permitted by statutory regulation or exceeds the permitted use, you will need to obtain permission directly from the copyright holder. To view a copy of this licence, visit http://creativecommons.org/licenses/by/4.0/.

References

1. Greenwood N. N., Gibb T. C.: Other Transition-metal Elements. In: N. N. Greenwood, T. C. Gibb) (eds.) Mössbauer Spectroscopy, pp 493–535. Dordrecht: Springer Netherlands (1971)
2. Wagner, F., Zahn, U.: Mssbauer isomer shifts, hyperfine interactions, and magnetic hyperfine anomalies in compounds of iridium. Z. Physik **233**(1), 1–20 (1970). https://doi.org/10.1007/BF01396512
3. Perlow, G.J., et al.: Hyperfine Anomaly in Ir193 by Mössbauer Effect, and its application to determination of the Orbital Part of Hyperfine Fields. Phys. Rev. Lett. **23**(13), 680–682 (1969). https://doi.org/10.1103/PhysRevLett.23.680
4. Alexeev, P., et al.: Nuclear resonant scattering from 193Ir as a probe of the electronic and magnetic properties of iridates. Sci. Rep. **9**(1), 5097 (2019). https://doi.org/10.1038/s41598-019-41130-3
5. Yang, C.-H., et al.: Blue-emitting heteroleptic iridium(III) complexes suitable for high-efficiency phosphorescent OLEDs. Angewandte Chemie **46**(14), 2418–2421 (2007). https://doi.org/10.1002/anie.200604733. (International ed. in English)
6. Reddy, M., Bejoymohandas, K.S.: Evolution of 2, 3′-bipyridine class of cyclometalating ligands as efficient phosphorescent iridium(III) emitters for applications in organic light emitting diodes. J. Photochem. Photobiol. C **29**, 29–47 (2016). https://doi.org/10.1016/j.jphotochemrev.2016.10.001
7. Dragonetti, C., et al.: Simple novel cyclometallated iridium complexes for potential application in dye-sensitized solar cells. Inorg. Chim. Acta **388**, 163 (2012). https://doi.org/10.1016/j.ica.2012.03.028
8. Day J. I. et al.: Advances in photocatalysis: a microreview of visible light mediated ruthenium and iridium catalyzed organic transformations. Org. Process Res. Dev. **20**(7), 1156–1163 (2016). https://doi.org/10.1021/acs.oprd.6b00101
9. McDaniel, N.D., et al.: Cyclometalated iridium(III) Aquo complexes: Efficient and tunable catalysts for the homogeneous oxidation of water. J. Am. Chem. Soc. **130**(1), 210–217 (2008). https://doi.org/10.1021/ja074478f
10. Hull, J.F., et al.: Highly active and robust Cp* iridium complexes for catalytic water oxidation. J. Am. Chem. Soc. **131**(25), 8730–8731 (2009). https://doi.org/10.1021/ja901270f
11. Bismuto, A., et al.: CCDC 1913379: Experimental crystal structure determination. Camb. Crystallographic Data Centre (2019). https://doi.org/10.5517/ccdc.csd.cc2270x8
12. Taguchi, K., et al.: An efficient direct alpha-alkylation of ketones with primary alcohols catalyzed by ir(cod)Cl2/PPh3/KOH system without solvent. J. Am. Chem. Soc. **126**(1), 72–73 (2004). https://doi.org/10.1021/ja037552c
13. Sakaguchi, S., et al.: Iridium-catalyzed transfer hydrogenation of alpha,beta-unsaturated and saturated carbonyl compounds with 2-propanol. J. Org. Chem. **66**(13), 4710–4712 (2001). https://doi.org/10.1021/jo0156722
14. Okimoto, Y., et al.: Development of a highly efficient catalytic method for synthesis of vinyl ethers. J. Am. Chem. Soc. **124**(8), 1590–1591 (2002). https://doi.org/10.1021/ja0173932

15. Morita, M., et al.: One-Pot synthesis of gamma,delta-unsaturated carbonyl compounds from allyl alcohols and vinyl or isopropenyl acetates catalyzed by IrCl(cod)2. J. Org. Chem. **71**(16), 6285–6286 (2006). https://doi.org/10.1021/jo060860j
16. Ishii, Y., Sakaguchi, S.: A novel catalysis of [{IrCl(Cod)} 2] Complex in Organic syntheses. BCSJ **77**(5), 909–920 (2004). https://doi.org/10.1246/bcsj.77.909
17. Crabtree, R.H., Morris, G.E.: Some diolefin complexes of iridium(I) and a trans-influence series for the complexes [IrCl(cod)L]. J. Organomet. Chem. **135**(3), 395–403 (1977). https://doi.org/10.1016/S0022-328X(00)88091-2
18. Kiyooka, S., et al.: [IrCl(cod)]2-catalyzed direct oxidative esterification of aldehydes with alcohols. Tetrahedron **63**(51), 12695–12701 (2007). https://doi.org/10.1016/j.tet.2007.10.003
19. Stęsik, K., et al.: Hydrosilylation of Carbonyl compounds Catalyzed by Iridium(I) complexes with (–)-Menthol-based phosphorus(III) ligands. Chem. Cat. Chem. **15**(9), (2023). https://doi.org/10.1002/cctc.202201510
20. Rahaman, S.W., et al.: The cyclooctadiene ligand in [IrCl(COD)] 2 is hydrogenated under transfer hydrogenation conditions: A study in the presence of PPh 3 and a strong base in isopropanol. J. Organomet. Chem. **829**, 14–21 (2017). https://doi.org/10.1016/j.jorganchem.2016.10.009
21. Srinivas, V., et al.: Iridium-Catalyzed Hydrosilylation of Sulfur-Containing olefins. Org. Lett. **20**(1), 12–15 (2018). https://doi.org/10.1021/acs.orglett.7b02940
22. Hesp, K.D., et al.: Ir(COD)Cl2 as a catalyst precursor for the intramolecular hydroamination of unactivated alkenes with primary amines and secondary alkyl- or arylamines: A combined catalytic, mechanistic, and computational investigation. J. Am. Chem. Soc. **132**(1), 413–426 (2010). https://doi.org/10.1021/ja908316n
23. Tuczek, F., et al.: 193 ir Mössbauer investigations of Iridium-C 60 adducts. Fullerene Sci. Technol. **5**(2), 443–452 (1997). https://doi.org/10.1080/15363839708012003
24. Gál, M., et al.: Mössbauer magnetization and nuclear magnetic resonance measurements on some iridium(I) complexes with fullerene ligands. J. Radioanal Nucl. Chem. **260**(1), 133–142 (2004). https://doi.org/10.1023/B:JRNC.0000027072.00903.fe
25. Chen, D., et al.: Luminescent Iridium(III) complexes supported by a tetradentate trianionic ligand Scaffold with mixed O, N, and C donor atoms: Synthesis, structures, Photophysical Properties, and material applications. Organometallics **36**(7), 1331–1344 (2017). https://doi.org/10.1021/acs.organomet.7b00038
26. Sturhahn, W.: CONUSS and PHOENIX: Evaluation of nuclear resonant scattering data. Hyperfine Interact **125**(1/4), 149–172 (2000). https://doi.org/10.1023/A:1012681503686
27. Reed, A.E., Curtiss, L.A., Weinhold, F.: Intermolecular interactions from a natural bond orbital, donor-acceptor viewpoint. Chem. Rev. **88**(6), 899–926 (1988). https://doi.org/10.1021/cr00088a005
28. Frisch, M.J., Trucks, G.W., Schlegel, H.B., Scuseria, G.E., Robb, M.A., Cheeseman, J.R., Scalmani, G., Barone, V., Petersson, G.A., Nakatsuji, H., Li, X., Caricato, M., Marenich, A.V., Bloino, J., Janesko, B.G., Gomperts, R., Mennucci, B., Hratchian, H.P., Ortiz, J.V., Izmaylov, A.F., Sonnenberg, J.L., Williams-Young, D., Ding, F., Lipparini, F., Egidi, F., Goings, J., Peng, B., Petrone, A., Henderson, T., Ranasinghe, D., Zakrzewski, V.G., Gao, J., Rega, N., Zheng, G., Liang, W., Hada, M., Ehara, M., Toyota, K., Fukuda, R., Hasegawa, J., Ishida, M., Nakajima, T., Honda, Y., Kitao, O., Nakai, H., Vreven, T., Throssell, K., Montgomery Jr., J.A., Peralta, J.E., Ogliaro, F., Bearpark, M.J., Heyd, J.J., Brothers, E.N., Kudin, K.N., Staroverov, V.N., Keith, T.A., Kobayashi, R., Normand, J., Raghavachari, K., Rendell, A.P., Burant, J.C., Iyengar, S.S., Tomasi, J., Cossi, M., Millam, J.M., Klene, M., Adamo, C., Cammi, R., Ochterski, J.W., Martin, R.L., Morokuma, K., Farkas, O., Foresman, J.B., Fox, D.J.: Gaussian 16 Rev. C.01. Gaussian Inc. Wallingford CT (2016)
29. Grimme, S., et al.: A consistent and accurate ab initio parametrization of density functional dispersion correction (DFT-D) for the 94 elements H-Pu. J. Chem. Phys. **132**(15), 154104 (2010). https://doi.org/10.1063/1.3382344
30. Weigend, F., Ahlrichs, R.: Balanced basis sets of split valence, triple zeta valence and quadruple zeta valence quality for H to rn: Design and assessment of accuracy. Phys. Chem. Chem. Phys. PCCP **7**(18), 3297–3305 (2005). https://doi.org/10.1039/b508541a
31. Weigend, F.: Accurate coulomb-fitting basis sets for H to Rn. Phys. Chem. Chem. Phys. **8**(9), 1057–1065 (2006). https://doi.org/10.1039/b515623h
32. Neese, F., et al.: The ORCA quantum chemistry program package. J. Chem. Phys. **152**(22), 224108 (2020). https://doi.org/10.1063/5.0004608
33. Pantazis, D.A., et al.: All-Electron Scalar relativistic basis sets for third-row transition metal atoms. J. Chem. Theory Comput. **4**(6), 908–919 (2008). https://doi.org/10.1021/ct800047t

34. Kaneko, M., Nakashima, S.: Density functional theory study on the 193Ir Mössbauer Spectroscopic parameters of Vaska's complexes and their oxidative adducts. Inorg. Chem. **60**(17), 12740–12752 (2021). https://doi.org/10.1021/acs.inorgchem.1c00239
35. Nieuwpoort, W.C., et al.: Calibration constant for Fe57 Mössbauer isomer shifts derived from ab initio self-consistent-field calculations on octahedral Fe F6 and Fe (CN)6 clusters. Phys. Rev. B **17**(1), 91–98 (1978). https://doi.org/10.1103/PhysRevB.17.91
36. Han, W.-G., et al.: DFT calculations of 57Fe Mössbauer isomer shifts and quadrupole splittings for iron complexes in polar dielectric media: Applications to methane monooxygenase and ribonucleotide reductase. J. Comput. Chem. **27**(12), 1292–1306 (2006). https://doi.org/10.1002/jcc.20402
37. Sinnecker, S., et al.: Performance of nonrelativistic and quasi-relativistic hybrid DFT for the prediction of electric and magnetic hyperfine parameters in 57Fe Mössbauer Spectra. Inorg. Chem. **44**(7), 2245–2254 (2005). https://doi.org/10.1021/ic048609e
38. Wagner, F.E., et al.: Mössbauer study of pentammine and pyridine complexes of iridium. Chem. Phys. **4**(2), 284–288 (1974). https://doi.org/10.1016/0301-0104(74)80095-9
39. Gütlich, P., et al.: Mössbauer spectroscopy and transition metal chemistry: fundamentals and applications. Springer, Berlin, Heidelberg (2011)

Publisher's Note Springer Nature remains neutral with regard to jurisdictional claims in published maps and institutional affiliations.